POLITECNICO DI TORINO
Repository ISTITUZIONALE

Bimodal Resonance Phenomena—Part I: Generalized Fabry–Pérot Interferometers

Original
Bimodal Resonance Phenomena—Part I: Generalized Fabry–Pérot Interferometers / Orta, R., Tibaldi, A., Debernardi, P.. - In: IEEE JOURNAL OF QUANTUM ELECTRONICS. - ISSN 0018-9197. - 52:12(2016), pp. 1-8. [10.1109/JQE.2016.2623270]

Availability:
This version is available at: 11583/2657916 since: 2018-11-08T11:05:16Z

Publisher:
IEEE

Published
DOI:10.1109/JQE.2016.2623270

Terms of use:

This article is made available under terms and conditions as specified in the corresponding bibliographic description in the repository

Publisher copyright
IEEE postprint/Author's Accepted Manuscript

©2016 IEEE. Personal use of this material is permitted. Permission from IEEE must be obtained for all other uses, in any current or future media, including reprinting/republishing this material for advertising or promotional purposes, creating new collecting works, for resale or lists, or reuse of any copyrighted component of this work in other works.

(Article begins on next page)

08 November 2026

Bimodal Resonance Phenomena. Part I: Generalized Fabry-Pérot Interferometers

Renato Orta, *Senior Member, IEEE*, Alberto Tibaldi, and Pierluigi Debernardi

***Abstract*—The operation of several optical components, such as high-contrast gratings, is based on the interference between two oscillation modes. Therefore, this paper is devoted to the complete characterization of bimodal Fabry-Pérot interferometers, which can effectively model such two-mode interactions. Thanks to a novel parametrization of the mirror scattering matrices, this paper presents for the first time explicit expressions of the bimodal interferometer response, proving phenomena such as 100% reflection peaks, and predicting their positions. For this reason this work, which complements -rather than replaces- the existing numerical techniques, provides a completely new perspective on high-contrast gratings.**

***Index Terms*—Fabry-Pérot interferometers, multimode waveguides, scattering parameters, resonance**

I. Introduction

RESONANCE phenomena have been observed and discussed in many subjects such as acoustics, optics, chemistry, elasticity or quantum mechanics. Being this topic so interdisciplinary and the related literature consequently vast, it is impossible to provide a comprehensive bibliography or even to establish a uniform writing style.

As an example, the electrical engineering community historically invested much effort into the characterization of resonant devices ranging from lumped circuits to distributed resonators. This is the case of *RCL* circuits, which have been described so effectively to allow for the implementation of the most disparate frequency responses with analytic synthesis procedures [1]. Distributed parameter single-mode resonators, such as the Fabry-Pérot interferometer (FPI), are textbook material as well, since their design-oriented analysis can be carried out with straightforward calculations [2].

A natural sequel of this topic is the characterization of bimodal cavities. Remarkably, high-contrast gratings (HCGs) fall into this category. HCGs have been largely adopted as compact mirrors [3]–[10], exhibiting reflectivity higher than 99.9% over an ultra broad band. Particularly interesting is the presence of 100% reflectivity peaks, which appear as the key to understand the wideband reflectivity and have been explained with interference principles [3], [11]. HCGs consist of a periodic arrangement of dielectric bars having refractive index much higher than the surrounding material [3]. The cavity can be identified as the bar region included within the two interfaces with free-space, which act as partially transparent mirrors.

An alternative application concerns very high Q compact resonators with surface-normal optical coupling [12], [13]. In this context, particular attention has been devoted to the presence of resonances in their response, which exhibits quick zero-one transitions, commonly referred to as Fano resonances (see, *e.g.*, [14, Fig. 3]). These have been attributed to interference phenomena occurring between the incident field and leaky waves propagating along the grating [15]–[20]. However, to the best of our knowledge, no analytic expressions for the positions of the zeros and ones of the response have been reported in the literature.

Of course, these phenomena can be easily simulated by means of numerical models. With reference to electromagnetic periodic structures, finite difference [21], finite element [22] or spectral element [23] methods have been successfully employed to analyze devices with arbitrary dielectric profiles. Another class of numerical schemes is based on modal methods, such as the popular rigorous coupled wave analysis (RCWA) [24], [25] or its following developments [26]. While the pros of the former methods are the flexibility in the description of the geometry, their results can be hardly interpreted physically. Instead, since the latter techniques exploit physical mechanisms such as propagation in homogeneous regions, their intermediate results (*e.g.* scattering matrices of interfaces) provide more insight into the device operation.

Similar arguments hold for the field of microwaves as well. The feed chain of high-throughput satellites consists of metallic waveguide components that may handle power of the order of several kilowatts [27]. In this framework, dual-mode E-plane stub filters resulted as very good candidates for high power handling [28]. These devices have been extensively characterized by means of numerical techniques such as the mode-matching methods [29], the boundary integral resonant mode expansion method (BI-RME) [30] or the spectral element method [31].

All the aforementioned structures are characterized by the presence of one propagating mode in their outer regions (*e.g.* free-space for HCGs or the input waveguide for stub filters) and two propagating modes in the inner cavities, in their operation frequency range. For this reason, inspired by [3], in this paper we developed a novel framework aimed at describing the behavior of bimodal FPIs. This is obtained through an extension of the analytic formulas available for the single-mode case: the response of a generic dual-mode resonator is decomposed into the sum of two single-mode

R. Orta is with the Department of Electronics and Telecommunications, Politecnico di Torino, Turin, 10129 Italy, and with IEIIT-CNR; e-mail: renato.orta@polito.it

A. Tibaldi and P. Debernardi are with the Consiglio Nazionale delle Ricerche (CNR), Istituto di Elettronica e di Ingegneria dell'Informazione e delle Telecomunicazioni (IEIIT), 10129 Turin, Italy.

Manuscript received August 2, 2016; revised October 14, 2016; accepted October 18, 2016.

responses. A major breakthrough, however, consists in a new parametrization of the mirror scattering matrices, leading to analytic expressions for the FPI reflection and transmission responses. The resulting abstract description allows to predict all the possible features of an arbitrary device compliant with the bimodal FPI concept. For example, thanks to our parametrization, it is possible to prove that the response of a bimodal FPI has always a 100% reflectivity peak. Explicit inverse formulas are obtained, allowing to evaluate the model parameters from the response of real devices. Such expressions have been used to produce a case study based on a high-contrast grating.

This is the first of a series of three papers devoted to the analysis and design of HCGs. The approach introduced here will be applied in Part II to characterize the resonance properties of HCGs. A successive work will deal with the broad-band reflectivity features of HCGs.

II. Review of single-mode interferometers

In this section the properties of the classic Fabry-Pérot interferometer (FPI) are briefly reviewed and re-formulated in view of the discussion of the bimodal case. A FPI consists of two partially reflecting mirrors separated by a distance L; its equivalent circuit is shown in Fig. 1, where only the first transmission line has to be considered. Let ϑ_1 indicate the phase shift introduced by the separation of the mirrors, which are described with their 2×2 scattering matrices $\overline{\mathbf{S}}'$, $\overline{\mathbf{S}}''$; the overbar denotes the junction scattering matrix. The input reflection coefficient is

$$S_{11} = \overline{S}'_{11} + \frac{\overline{S}''_{11}\overline{S}'_{21}\overline{S}'_{12}\mathrm{e}^{-\mathrm{j}2\vartheta_1}}{1-\overline{S}'_{22}\overline{S}''_{11}\mathrm{e}^{-\mathrm{j}2\vartheta_1}}. \tag{1}$$

Mirrors are assumed to be reciprocal, lossless and non-dispersive, so that their scattering matrices are symmetrical, unitary and frequency independent, leading to the well known parametrization

$$\overline{\mathbf{S}} = \begin{bmatrix} \mathrm{e}^{\mathrm{j}\phi_{11}}\cos\gamma & \mathrm{j}\mathrm{e}^{\mathrm{j}\phi_{12}}\sin\gamma \\ \mathrm{j}\mathrm{e}^{\mathrm{j}\phi_{12}}\sin\gamma & \mathrm{e}^{\mathrm{j}\phi_{22}}\cos\gamma \end{bmatrix}, \tag{2}$$

with $\phi_{12} = (\phi_{11}+\phi_{22})/2 \pm \pi$, and $0 \le \gamma \le \pi/2$. With this, the previous equation can be rewritten as

$$S_{11} = \mathrm{e}^{\mathrm{j}\phi'_{11}}\left(\frac{\cos\gamma' - \cos\gamma''\,\mathrm{e}^{-\mathrm{j}2\vartheta_{1,\mathrm{eq}}}}{1-\cos\gamma'\cos\gamma''\,\mathrm{e}^{-\mathrm{j}2\vartheta_{1,\mathrm{eq}}}}\right) = \mathcal{C}(\vartheta_{1,\mathrm{eq}}), \tag{3}$$

where $\vartheta_{1,\mathrm{eq}} = \vartheta_1 - (\phi''_{11}+\phi'_{22})/2$ and ϕ_{ij} are the phases of the scattering parameters. When $\vartheta_{1,\mathrm{eq}} \in [0, 2\pi]$, the quantity within the parentheses traces twice a circle in the complex plane, with center on the real axis and intersecting it in the points

$$|S_{11}|^{\max}_{\min} = \frac{|\cos\gamma' \pm \cos\gamma''|}{1 \pm \cos\gamma'\cos\gamma''}.$$

Indeed, (3) is a Möbius transformation mapping the unit circle $\mathrm{e}^{-\mathrm{j}2\vartheta_{1,\mathrm{eq}}}$ into the circle just described. Note that $|\overline{S}'_{22}| = |\overline{S}'_{11}|$. If the two mirrors are equal, the circle passes through the origin. This circle is then rotated by ϕ'_{11} because of the prefactor. It is useful to remark that $\cos\gamma'\cos\gamma''\mathrm{e}^{-j2\vartheta_{1,\mathrm{eq}}}$ is commonly referred to as loop gain and $2\vartheta_{1,\mathrm{eq}}$ as round-trip phase shift.

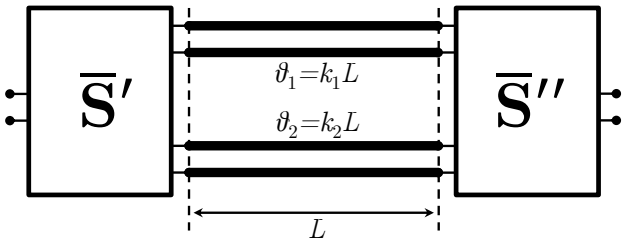

Fig. 1. Equivalent circuit of a bimodal FPI. The left and right scattering matrices are connected through two transmission lines with length L and with propagation constants k_1, k_2.

The transmission coefficient of the FPI is

$$S_{21} = \frac{\overline{S}'_{21}\overline{S}''_{21}\mathrm{e}^{-\mathrm{j}\vartheta_1}}{1-\overline{S}'_{22}\overline{S}''_{11}\mathrm{e}^{-\mathrm{j}2\vartheta_1}} = \\ = \mathrm{e}^{-\mathrm{j}\frac{\phi'_{11}+\phi''_{22}}{2}}\frac{\sin\gamma'\sin\gamma''\mathrm{e}^{-\mathrm{j}\vartheta_{1,\mathrm{eq}}}}{1-\cos\gamma'\cos\gamma''\mathrm{e}^{-\mathrm{j}2\vartheta_{1,\mathrm{eq}}}}. \tag{4}$$

By rewriting the previous equation in the form

$$S_{21}^{-1} = \frac{1}{\overline{S}'_{21}\overline{S}''_{21}}\mathrm{e}^{\mathrm{j}\vartheta_1} - \frac{\overline{S}'_{22}\overline{S}''_{11}}{\overline{S}'_{21}\overline{S}''_{21}}\mathrm{e}^{-\mathrm{j}\vartheta_1} = \\ = A\mathrm{e}^{\mathrm{j}\vartheta_1} + B\mathrm{e}^{-\mathrm{j}\vartheta_1} = \mathcal{E}(\vartheta_1), \tag{5}$$

it can be noted that the curves of S_{21} in the complex plane are inverse of ellipses $\mathcal{E}(\vartheta_1)$ with semiaxes

$$|\mathcal{E}|_{\max} = |A| + |B| = \frac{1+\cos\gamma'\cos\gamma''}{\sin\gamma'\sin\gamma''}$$

$$|\mathcal{E}|_{\min} = |A| - |B| = \frac{1-\cos\gamma'\cos\gamma''}{\sin\gamma'\sin\gamma''}$$

leading to

$$|S_{21}|^{\max}_{\min} = \frac{\sin\gamma'\sin\gamma''}{1 \mp \cos\gamma'\cos\gamma''}$$

obtained for $\vartheta_{1,\mathrm{eq}} = n\pi$ and $(n+1/2)\pi$, respectively. Note that $|S_{21}|_{\max} = 1$ only if the two mirrors are equal, as well known.

III. Bimodal interferometers

In a bimodal FPI the field incident on the mirror couples to two propagating modes in the cavity. This is described by the circuit sketched in Fig. 1, where the two transmission lines with propagation constants k_1, k_2 connect the internal ports of the 3×3 mirror scattering matrices. The distinction of inner and outer regions suggests to partition the scattering matrices as

$$\overline{\mathbf{S}}' = \begin{bmatrix} \overline{S}'_{\mathrm{oo}} & \overline{\mathbf{S}}'_{\mathrm{oi}} \\ \overline{\mathbf{S}}'_{\mathrm{io}} & \overline{\mathbf{S}}'_{\mathrm{ii}} \end{bmatrix} \qquad \overline{\mathbf{S}}'' = \begin{bmatrix} \overline{\mathbf{S}}''_{\mathrm{ii}} & \overline{\mathbf{S}}''_{\mathrm{io}} \\ \overline{\mathbf{S}}''_{\mathrm{oi}} & \overline{S}''_{\mathrm{oo}} \end{bmatrix}, \tag{6}$$

where $\overline{\mathbf{S}}_{\mathrm{ii}}$ is the 2×2 mirror reflection matrix seen from inside the resonator, the transmissions $\overline{\mathbf{S}}_{\mathrm{oi}}$ and $\overline{\mathbf{S}}_{\mathrm{io}}$ are vectors, and the reflection coefficient at the outer port $\overline{S}_{\mathrm{oo}}$ is a scalar. Let $\vartheta_1 = k_1 L$, $\vartheta_2 = k_2 L$ be the electrical lengths of the cavity for

the two modes, as indicated in Fig. 1. From these, we define the two equivalent variables

$$\overline{\vartheta} = \frac{\vartheta_1 + \vartheta_2}{2}$$
$$\Delta\vartheta = \vartheta_1 - \vartheta_2.$$

Then, the internal reference planes are shifted to the middle of the cavity by means of the matrix defined by

$$\mathrm{diag}\{\mathrm{e}^{-\mathrm{j}\frac{\vartheta_1}{2}}, \mathrm{e}^{-\mathrm{j}\frac{\vartheta_2}{2}}\} = \mathrm{e}^{-\mathrm{j}\frac{\overline{\vartheta}}{2}}\mathrm{diag}\{\mathrm{e}^{-\mathrm{j}\frac{\Delta\vartheta}{4}}, \mathrm{e}^{\mathrm{j}\frac{\Delta\vartheta}{4}}\} = \mathrm{e}^{-\mathrm{j}\frac{\overline{\vartheta}}{2}}\mathbf{E}.$$

Finally, the two blocks are cascaded, obtaining the reflection and transmission coefficients

$$S_{11} = \overline{S}'_{\mathrm{oo}} + \mathrm{e}^{-\mathrm{j}2\overline{\vartheta}}\overline{\mathbf{S}}'_{\mathrm{oi}}\mathbf{E}^2\,\overline{\mathbf{S}}''_{\mathrm{ii}}\,\mathbf{E}\left[\mathbf{I} - \mathrm{e}^{-\mathrm{j}2\overline{\vartheta}}\mathbf{T}\right]^{-1}\mathbf{E}\,\overline{\mathbf{S}}'_{\mathrm{io}}, \quad (7)$$

$$S_{21} = \mathrm{e}^{-\mathrm{j}2\overline{\vartheta}}\overline{\mathbf{S}}''_{\mathrm{oi}}\mathbf{E}\left[\mathbf{I} - \mathrm{e}^{-\mathrm{j}2\overline{\vartheta}}\mathbf{T}\right]^{-1}\mathbf{E}\,\overline{\mathbf{S}}'_{\mathrm{io}}, \quad (8)$$

where $\mathbf{T}$ is defined as

$$\mathbf{T} = \mathbf{E}\,\overline{\mathbf{S}}'_{\mathrm{ii}}\mathbf{E}^2\,\overline{\mathbf{S}}''_{\mathrm{ii}}\mathbf{E} \quad (9)$$

and the factorization of the $\mathrm{e}^{-\mathrm{j}2\overline{\vartheta}}$ term can be seen as the result of the phase-unwrapping of the loop gain matrix. In general, $\mathbf{T}$ is not symmetric, unless $\overline{\mathbf{S}}'_{\mathrm{ii}} = \overline{\mathbf{S}}''_{\mathrm{ii}}$.

In order to better understand the general behavior of the device it is convenient to use the oscillation modes as a basis in the cavity region, so that the loop gain matrix becomes diagonal. This approach has been adopted also in [3], where a connection was noted between the response and the phases of the eigenvalues of the loop gain. In order to define an idealized framework of operation, it is useful to assume that the mirror scattering matrices and $\Delta\vartheta$ are independent of frequency. In this way it will be possible to carry out explicitely a complete analysis of the structure.

The resonant factor of the previous equations can be written as

$$\left(\mathbf{I} - \mathrm{e}^{-\mathrm{j}2\overline{\vartheta}}\mathbf{T}\right)^{-1} = \mathbf{V}\begin{bmatrix}\dfrac{1}{1-\mu_1\mathrm{e}^{-\mathrm{j}2\overline{\vartheta}}} & 0\\ 0 & \dfrac{1}{1-\mu_2\mathrm{e}^{-\mathrm{j}2\overline{\vartheta}}}\end{bmatrix}\mathbf{V}^{-1},$$

by exploiting the eigendecomposition of $\mathbf{T}$ (eigenvalues $\{\mu_i\}$ and eigenvector matrix $\mathbf{V}$). This does not depend on $\overline{\vartheta}$ (*i.e.* on frequency) thanks to the assumption of absence of dispersion of $\Delta\vartheta$. Then, by substituting the last expression in (8), the transmission coefficient of the whole device can be decomposed as

$$S_{21} = S_{21}^{(1)} + S_{21}^{(2)}, \quad (10)$$

where the k-th contribution

$$S_{21}^{(k)} = \frac{\widetilde{S}''_{\mathrm{oi},k}\,\widetilde{S}'_{\mathrm{io},k}\mathrm{e}^{-\mathrm{j}\overline{\vartheta}}}{1-\mu_k\mathrm{e}^{-\mathrm{j}2\overline{\vartheta}}}$$

has the same expression as in (4), *i.e.* the reciprocal of an ellipse $\mathcal{E}_k(\overline{\vartheta})$. Here, $\widetilde{\mathbf{S}}'_{\mathrm{io}}$, $\widetilde{\mathbf{S}}''_{\mathrm{oi}}$ are the transmission coefficients from the external port to the middle of the cavity (and viceversa), expressed in the cavity mode basis:

$$\widetilde{\mathbf{S}}'_{\mathrm{io}} = \mathbf{V}^{-1}\mathbf{E}\,\overline{\mathbf{S}}'_{\mathrm{io}} = \begin{bmatrix}\widetilde{S}'_{\mathrm{io},1} & \widetilde{S}'_{\mathrm{io},2}\end{bmatrix}^{\mathrm{T}}$$
$$\widetilde{\mathbf{S}}''_{\mathrm{oi}} = \overline{\mathbf{S}}''_{\mathrm{oi}}\mathbf{E}\,\mathbf{V} = \begin{bmatrix}\widetilde{S}''_{\mathrm{oi},1} & \widetilde{S}''_{\mathrm{oi},2}\end{bmatrix}.$$

Similarly, the reflection coefficient can be decomposed into its modal constituents by substituting the eigendecomposition in (7), leading to

$$S_{11} = \overline{S}'_{\mathrm{oo}} + S_{11}^{(1)} + S_{11}^{(2)}, \quad (11)$$

where each contribution

$$S_{11}^{(k)} = P_k\,\widetilde{S}'_{\mathrm{io},k}\frac{\mathrm{e}^{-\mathrm{j}2\overline{\vartheta}}}{1-\mu_k\mathrm{e}^{-\mathrm{j}2\overline{\vartheta}}}$$

is, just like (3), a Möbius transformation mapping circles into circles. Here, P_k are the components of the row vector

$$\mathbf{P} = \begin{bmatrix}P_1 & P_2\end{bmatrix} = \widetilde{\mathbf{S}}'_{\mathrm{oi}}\widetilde{\mathbf{S}}''_{\mathrm{ii}}.$$

Equations (10) and (11) state that the reflection and transmission responses of a bimodal interferometer can be decomposed into two single-mode responses, allowing to exploit the results reviewed in Section II. The transmission coefficient can be written as

$$S_{21} = \frac{1}{\mathcal{E}_1(\overline{\vartheta})} + \frac{1}{\mathcal{E}_2(\overline{\vartheta})} = \frac{\mathcal{E}_1(\overline{\vartheta}) + \mathcal{E}_2(\overline{\vartheta})}{\mathcal{E}_1(\overline{\vartheta})\,\mathcal{E}_2(\overline{\vartheta})}, \quad (12)$$

where $\mathcal{E}_k$ is an ellipse as in (5). Therefore $S_{21} = 0$ if

$$\mathcal{E}_1(\overline{\vartheta}) + \mathcal{E}_2(\overline{\vartheta}) = 0,$$

which can be expanded as

$$(A_1 + A_2)\mathrm{e}^{\mathrm{j}\overline{\vartheta}} - (B_1 + B_2)\mathrm{e}^{-\mathrm{j}\overline{\vartheta}} = 0.$$

and the coefficients A_k, B_k are defined in (5). The sum of two ellipses is another ellipse, and it is clear that this equation has real solutions only if

$$|A_1 + A_2| = |B_1 + B_2|\,, \quad (13)$$

which means that the resulting ellipse degenerates into a straight line through the origin. Indeed, in this case:

$$\mathcal{E}_1(\overline{\vartheta}) + \mathcal{E}_2(\overline{\vartheta}) = |A_1 + A_2|\,\mathrm{e}^{\mathrm{j}\frac{\alpha}{2}}\left[\mathrm{e}^{\mathrm{j}\left(\overline{\vartheta}-\frac{\alpha}{2}\right)} + \mathrm{e}^{-\mathrm{j}\left(\overline{\vartheta}-\frac{\alpha}{2}\right)}\right] =$$
$$= 2\,|A_1 + A_2|\,\mathrm{e}^{\mathrm{j}\frac{\alpha}{2}}\cos\left(\overline{\vartheta} - \frac{\alpha}{2}\right),$$

where

$$\alpha = \angle(B_1 + B_2) - \angle(A_1 + A_2).$$

Hence S_{21} has a zero at

$$\overline{\vartheta}_{\mathrm{z},21} = \frac{\pi}{2}(2n+1) + \frac{\alpha}{2}.$$

Condition (13) is always satisfied for lossless reciprocal devices, as will be rigorously proved by exploiting the parametrization introduced in the next section.

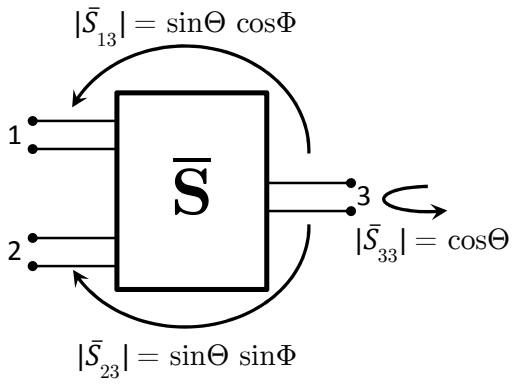

Fig. 2. Graphical representation of a lossless 3-ports device; 1 and 2 are the inner ports, whereas 3 is the outer one.

Similarly, for the zeros of the reflection coefficient, (11) is rewritten as

$$S_{11} = \overline{S}'_{\mathrm{oo}} + \frac{1}{\mathcal{C}_1} + \frac{1}{\mathcal{C}_2} = \frac{\overline{S}'_{\mathrm{oo}}\mathcal{C}_1\mathcal{C}_2 + \mathcal{C}_1 + \mathcal{C}_2}{\mathcal{C}_1\mathcal{C}_2},$$

where $\mathcal{C}_k$ is a circle as in (1). Setting this expression to zero leads to a fairly involved biquadratic equation in the unknown $\mathrm{e}^{-\mathrm{j}\overline{\vartheta}}$. It could be shown that its $\overline{\vartheta}$ roots can either lie on the real axis or exhibit an imaginary part, depending on the mirrors. As for S_{21}, more information can be achieved by exploiting the aforementioned matrix parametrization.

As it is clear from (10)-(11), the response poles are related to the eigenvalues of the loop gain matrix by

$$\overline{\vartheta}_{\mathrm{p},k} = \frac{1}{2\mathrm{j}}\ln\mu_k + n\pi. \tag{14}$$

IV. Parametrization of Unitary Symmetric 3×3 Scattering Matrices

In order to complete the details of the framework described in the previous sections in the very common case of lossless reciprocal devices, the properties of unitarity and symmetry are enforced on the mirror scattering matrices. Even though several works can be found in the literature that discuss the parametrization of generic unitary [32], [33] and also symmetric [34] matrices, the one proposed here for the first time lends itself to clear physical interpretations of its parameters when applied to the junction scattering matrices. Focusing on the scattering matrix of the second junction (6), 1 and 2 are chosen as the inner ports, and 3 is the outer one

$$\overline{\mathbf{S}} = \left[\begin{array}{c|c} \overline{\mathbf{S}}_{\mathrm{ii}} & \overline{\mathbf{S}}_{\mathrm{io}} \\ \hline \overline{\mathbf{S}}_{\mathrm{oi}} & \overline{S}_{\mathrm{oo}} \end{array}\right] = \left[\begin{array}{cc|c} \overline{S}_{11} & \overline{S}_{12} & \overline{S}_{13} \\ \overline{S}_{12} & \overline{S}_{22} & \overline{S}_{23} \\ \hline \overline{S}_{13} & \overline{S}_{23} & \overline{S}_{33} \end{array}\right], \tag{15}$$

where symmetry is enforced. The matrix contains six complex numbers but the unitarity condition $\overline{\mathbf{S}}\,\overline{\mathbf{S}}^{\mathrm{T}*} = \mathbf{I}$ imposes six constrains, so that in the end $\overline{\mathbf{S}}$ is uniquely defined by only six real parameters.

The parametrization is based on the following factorization [35]

$$\overline{\mathbf{S}} = \mathbf{H}\,\mathbf{A}\,\mathbf{H}^{\mathrm{T}}, \tag{16}$$

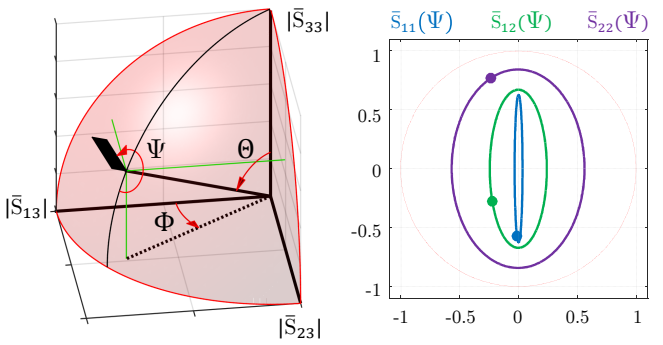

Fig. 3. Left: geometric interpretation of the junction scattering parameters in terms of a spherical coordinate system. The unit sphere is highlighted. Right: elements of the 2×2 submatrix $\overline{\mathbf{S}}''_{\mathrm{ii}}$. With running Ψ, they trace ellipses in the complex plane. In this example, which refers to the HCG studied in Part II, $\Theta = 62.55°$, $\Phi = 33.26°$; the dot markers indicate $\Psi = 246.02°$. The unit circle (red curve) has been added for reference.

where

$$\mathbf{A} = \mathrm{e}^{\mathrm{j}\alpha_1}\begin{bmatrix} \cos\alpha_2 & 0 & \mathrm{j}\sin\alpha_2 \\ 0 & 1 & 0 \\ \mathrm{j}\sin\alpha_2 & 0 & \cos\alpha_2 \end{bmatrix} \tag{17}$$

is unitary and symmetric,

$$\mathbf{H} = \left[\begin{array}{cc|c} h_{11} & h_{12} & 0 \\ h_{21} & h_{22} & 0 \\ \hline 0 & 0 & 1 \end{array}\right] \tag{18}$$

is unitary because such is its block $\mathbf{h}$ defined as

$$\mathbf{h} = \mathrm{e}^{-\mathrm{j}\frac{\alpha_4+\alpha_1}{2}}\begin{bmatrix} \mathrm{e}^{\mathrm{j}\alpha_5}\cos\alpha_3 & \mathrm{j}\mathrm{e}^{\mathrm{j}\alpha_6}\sin\alpha_3 \\ \mathrm{j}\mathrm{e}^{-\mathrm{j}\alpha_6}\sin\alpha_3 & \mathrm{e}^{-\mathrm{j}\alpha_5}\cos\alpha_3 \end{bmatrix}. \tag{19}$$

The physical interpretation of its parameters is eased by defining

$$\alpha_5 = \frac{1}{2}(-\Delta + \Psi) \qquad \alpha_6 = \frac{1}{2}(-\Delta - \Psi),$$

and by renaming the other α_i as follows

$$\alpha_1 = \varphi_{33} \qquad \alpha_2 = \Theta \qquad \alpha_3 = \Phi \qquad \alpha_4 = \varphi_{\mathrm{c}}.$$

Carrying out the matrix products in (16) the explicit expressions of the scattering matrix elements in terms of the parameters is obtained:

$$\begin{aligned}
\overline{S}_{11} &= \mathrm{e}^{-\mathrm{j}(\varphi_{\mathrm{c}}+\Delta)}\left[\mathrm{e}^{\mathrm{j}\Psi}\cos^2\Phi\cos\Theta - \mathrm{e}^{-\mathrm{j}\Psi}\sin^2\Phi\right] \\
\overline{S}_{22} &= \mathrm{e}^{-\mathrm{j}(\varphi_{\mathrm{c}}-\Delta)}\left[\mathrm{e}^{-\mathrm{j}\Psi}\cos^2\Phi - \mathrm{e}^{\mathrm{j}\Psi}\sin^2\Phi\cos\Theta\right] \\
\overline{S}_{12} &= \frac{1}{2}\mathrm{j}\mathrm{e}^{-\mathrm{j}\varphi_{\mathrm{c}}}\sin 2\Phi\left[\mathrm{e}^{-\mathrm{j}\Psi} + \mathrm{e}^{\mathrm{j}\Psi}\cos\Theta\right] \\
\overline{S}_{13} &= \mathrm{j}\mathrm{e}^{\mathrm{j}\frac{-\varphi_{\mathrm{c}}+\varphi_{33}+\Psi}{2}}\mathrm{e}^{-\mathrm{j}\frac{\Delta}{2}}\sin\Theta\cos\Phi \\
\overline{S}_{23} &= -\mathrm{e}^{\mathrm{j}\frac{-\varphi_{\mathrm{c}}+\varphi_{33}+\Psi}{2}}\mathrm{e}^{\mathrm{j}\frac{\Delta}{2}}\sin\Theta\sin\Phi \\
\overline{S}_{33} &= \mathrm{e}^{\mathrm{j}\varphi_{33}}\cos\Theta.
\end{aligned} \tag{20}$$

From the last three equations of (20) it can be seen that Θ and φ_{33} characterize the magnitude and phase of $\overline{S}_{33}$. Assuming a wave incident on port 3, the angle Φ controls the power partitioning between ports 1 and 2. The relationships

between the magnitudes of $\overline{S}_{13}$, $\overline{S}_{23}$ and $\overline{S}_{33}$ are shown in Fig. 2: clearly, if the junction is highly reflecting from port 3, it is poorly transmitting toward ports 1 and 2. Such unitarity constraint leads to the graphical interpretation depicted in Fig. 3(left). This figure shows a flag in a spherical coordinate system whose pole, of unit length, is oriented in the direction specified by the zenith and azimuth angles Θ and Φ. The projections on the axes x, y, z are the magnitudes of $\overline{S}_{13}$, $\overline{S}_{23}$, $\overline{S}_{33}$, respectively. The flag orientation, measured by Ψ, has no impact on the magnitudes of S_{i3}. This representation, which is suggested by the last three equations of (20), shows how our parametrization is a natural extension of (2) for the bimodal case.

Not so obvious is the relationship between $\overline{S}_{33}$ and the 2×2 sub-matrix $\overline{\mathbf{S}}_{\mathrm{ii}}$. The first three equations of (20) show that the square parentheses trace ellipses parametrized by Ψ. The additional phase factors are related to the position of the reference planes of ports 1 and 2: φ_{c} is a common phase factor, whereas Δ is a differential phase factor between the two ports. As an example, Fig. 3(right) shows possible values of the $\overline{\mathbf{S}}_{\mathrm{ii}}$ sub-matrix elements for a given choice of Θ and Φ. The phase factors outside the square parentheses have not been included.

V. Explicit expressions of S_{11}, S_{21} and their zeros

The parametrization introduced in Section IV is now applied to the reflection and transmission responses reported in Section III in order to obtain more explicit expressions. This opens up the possibility to perform a detailed study of the interferometer response. As it could be expected, the explicitation of (7) and (8) gives rise to very complicated expressions. For this reason the study is limited to symmetrical resonators, covering nevertheless a large variety of cases [3], so that only six parameters instead of twelve are required to describe the junctions.

First of all, from (7), (8) and (20), it is possible to prove the following property:

$$\begin{aligned} &S_{ij}(\overline{\vartheta}; \Theta, \Phi, \Psi, \Delta, \varphi_{\mathrm{c}}, \varphi_{33}, \Delta\vartheta) = \\ &= S_{ij}(\overline{\vartheta}_{\mathrm{eq}}; \Theta, \Phi, \Psi, 0, 0, 0, \Delta\vartheta_{\mathrm{eq}})\, \mathrm{e}^{\mathrm{j}\varphi_{33}}, \end{aligned} \tag{21}$$

where

$$\overline{\vartheta}_{\mathrm{eq}} = \overline{\vartheta} + \varphi_{\mathrm{c}} \qquad\qquad \Delta\vartheta_{\mathrm{eq}} = \Delta\vartheta + 2\Delta.$$

This means that the magnitudes of the FPI scattering parameters depend only on five quantities instead of eight; from now on, the subscript "eq" will be dropped to simplify the notation. The explicit expression of S_{21} is

$$S_{21} = \frac{N}{D} \mathrm{e}^{-\mathrm{j}\overline{\vartheta}} \mathrm{e}^{\mathrm{j}\varphi_{33}}, \tag{22}$$

where D is the determinant of $(\mathbf{I} - \mathrm{e}^{-\mathrm{j}2\overline{\vartheta}}\mathbf{T})$

$$D = c_{4\mathrm{d}} \mathrm{e}^{-\mathrm{j}4\overline{\vartheta}} + c_{2\mathrm{d}} \mathrm{e}^{-\mathrm{j}2\overline{\vartheta}} + 1,$$

and

$$\begin{aligned} c_{4\mathrm{d}} &= \cos^2\Theta \\ c_{2\mathrm{d}} &= \mathrm{e}^{-\mathrm{j}(2\Psi+\Delta\vartheta)} \left(p_4 \mathrm{e}^{\mathrm{j}4\Psi} + p_2 \mathrm{e}^{\mathrm{j}2\Psi} + p_0 \right), \end{aligned}$$

and

$$\begin{aligned} p_4 &= -\cos^2\Theta \left(\cos^2\Phi - \mathrm{e}^{\mathrm{j}\Delta\vartheta} \sin^2\Phi \right)^2 \\ p_2 &= \frac{1}{2} \left(1 + \mathrm{e}^{\mathrm{j}\Delta\vartheta} \right)^2 \cos\Theta \sin^2 2\Phi \\ p_0 &= -\left(\sin^2\Phi - \mathrm{e}^{\mathrm{j}\Delta\vartheta} \cos^2\Phi \right)^2. \end{aligned}$$

The numerator N is

$$N = -\frac{1}{2} \mathrm{e}^{-\mathrm{j}(\Psi + \Delta\vartheta/2)} \sin^2\Theta \left(c_{0\mathrm{n}} + c_{1\mathrm{n}} \mathrm{e}^{-\mathrm{j}2\overline{\vartheta}} \right), \tag{23}$$

with

$$\begin{aligned} c_{0\mathrm{n}} &= \mathrm{e}^{\mathrm{j}2\Psi} \left(1 - \mathrm{e}^{\mathrm{j}\Delta\vartheta} + \left(1 + \mathrm{e}^{\mathrm{j}\Delta\vartheta} \right) \cos 2\Phi \right) \\ c_{1\mathrm{n}} &= \left(1 - \mathrm{e}^{\mathrm{j}\Delta\vartheta} \right) - \left(1 + \mathrm{e}^{\mathrm{j}\Delta\vartheta} \right) \cos 2\Phi. \end{aligned}$$

The expression of the reflection coefficient S_{11} is

$$S_{11} = \frac{1}{D} \left(\cos\Theta\, \mathrm{e}^{-\mathrm{j}4\overline{\vartheta}} + c_{2\mathrm{n}} \mathrm{e}^{-\mathrm{j}2\overline{\vartheta}} + \cos\Theta \right) \mathrm{e}^{\mathrm{j}\varphi_{33}}, \tag{24}$$

where the denominator D is the same as in S_{21} and

$$c_{2\mathrm{n}} = t_2 \mathrm{e}^{\mathrm{j}2\Psi} + t_2^* \mathrm{e}^{-\mathrm{j}2\Psi} + t_0,$$

where

$$\begin{aligned} t_2 &= -\cos\Theta \left(\mathrm{e}^{-\mathrm{j}\frac{\Delta\vartheta}{2}} \cos^2\Phi - \mathrm{e}^{\mathrm{j}\frac{\Delta\vartheta}{2}} \sin^2\Phi \right)^2 \\ t_0 &= \frac{1}{2} (3 + \cos 2\Theta) \cos^2 \frac{\Delta\vartheta}{2} \sin^2 2\Phi. \end{aligned}$$

The zeros of the transmission coefficient are obtained from (23)

$$\mathrm{e}^{-\mathrm{j}2\overline{\vartheta}} = -\frac{c_{0\mathrm{n}}}{c_{1\mathrm{n}}},$$

and, by exploiting the expressions of these coefficients, we get

$$\overline{\vartheta}_{\mathrm{z},21} = -\Psi + \arctan\left(\frac{\tan(\Delta\vartheta/2)}{\cos 2\Phi} \right). \tag{25}$$

It can be seen that $\overline{\vartheta}_{\mathrm{z},21}$ is real for all values of the parameters, and this is the proof of (13). Therefore, every symmetrical bimodal FPI exhibits 100% reflection peaks. Note that this remarkable property is a consequence of the only hypotheses of absence of lossless and reciprocity of the structure.

Concerning the reflection coefficient, we find the zeros of S_{11} from (24). The solution of the biquadratic equation can be cast in the form

$$\overline{\vartheta}_{\mathrm{z},11} = \frac{1}{2} \arccos\left(-\frac{c_{2\mathrm{n}}}{2\cos\Theta} \right), \tag{26}$$

where $c_{2\mathrm{n}}$ is real. However the zeros are real only if

$$\left| \frac{c_{2\mathrm{n}}}{2\cos\Theta} \right| \leq 1. \tag{27}$$

If this condition is not satisfied, the zeros are complex conjugate.

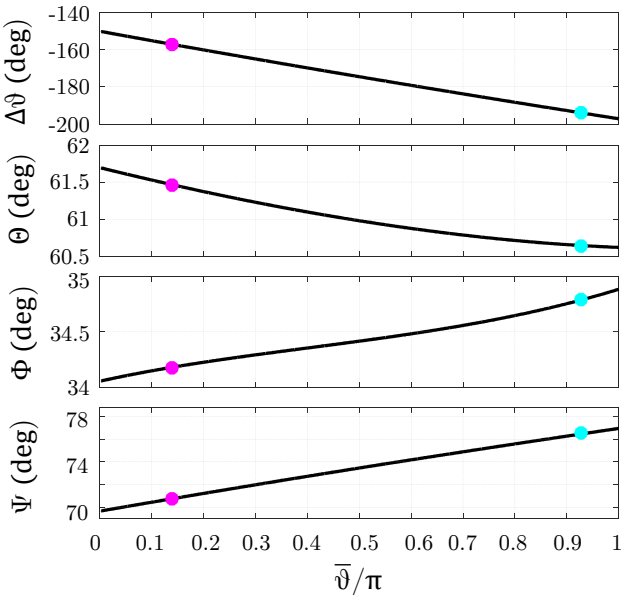

Fig. 4. Plots of the parameters $\Delta\vartheta$, Θ, Φ, Ψ of the high-contrast grating studied in [3, Fig. 6(b)], with $t_g = \Lambda$ and $\lambda \in [1.3, 1.6]\Lambda$. The junction $\overline{\mathbf{S}}$ parameters have been obtained with the RCWA. The dots indicate two specific frequencies, see Fig. 5

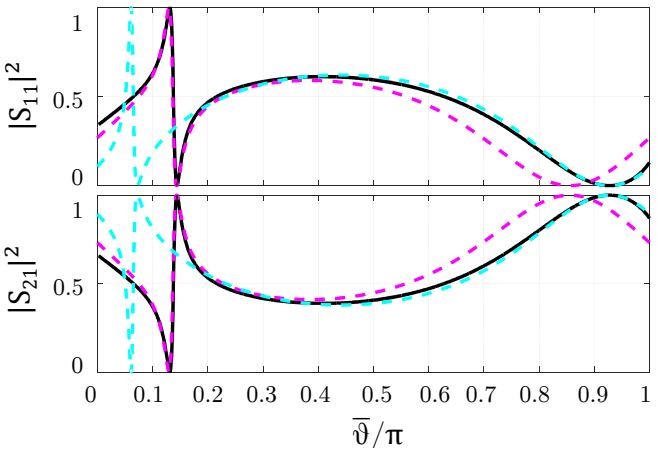

Fig. 5. Example of normal-incidence TE plane-wave response in reflection (top) and transmission (bottom) of a high-contrast grating from [3, Fig. 6(b)], with $t_g = \Lambda$ and $\lambda \in [1.3, 1.6]\Lambda$. The solid black curves are obtained with the RCWA, whereas the magenta and cyan dashed curves with (22), (24), for the parameter values indicated with the corresponding colors by the dot markers in Fig. 4.

VI. Inverse formulas and numerical example

In order to apply this theoretical framework to "real world devices" such as high-contrast gratings [3] or microwave stub filters [27], it is necessary to evaluate the parameters of (20) from the junction scattering matrix. A major advantage of our parametrization is the possibility to obtain explicit inverse formulas allowing the identification of the model without the numerical solution of non-linear equations. To this aim, starting from the last two equations of (20), one can write

$$\begin{aligned}\Theta &= \arccos(|\overline{S}_{33}|)\\ \varphi_{33} &= \arg\left(\overline{S}_{33}\right)\\ \Phi &= \arccos\left(\frac{|\overline{S}_{13}|}{\sin\Theta}\right) = \arcsin\left(\frac{|\overline{S}_{23}|}{\sin\Theta}\right).\end{aligned}$$

Then, a direct computation yields

$$\det\overline{\mathbf{S}}_{11} = \overline{S}_{11}\overline{S}_{22} - \overline{S}_{12}^2 = \mathrm{e}^{-\mathrm{j}2\varphi_c}\cos\Theta,$$

hence

$$\varphi_c = -\frac{1}{2}\arg\left(\frac{\det\overline{\mathbf{S}}_{ii}}{\cos\Theta}\right).$$

Finally, from the fourth and fifth equations,

$$\begin{aligned}\Delta &= (\arg(\overline{S}_{23}) - \arg(\overline{S}_{13})) - \frac{\pi}{2}\\ \Psi &= \arg(\overline{S}_{23}) + \arg(\overline{S}_{13}) + \varphi_c - \varphi_{33} - \frac{3\pi}{2}.\end{aligned} \tag{28}$$

These formulas complete the theoretical framework for the characterization of lossless reciprocal bimodal interferometers.

Figure 4 reports the parameters $\Delta\vartheta$, Θ, Φ, Ψ obtained by applying the inverse formulas to the junction scattering matrix $\overline{\mathbf{S}}$ of a high-contrast grating studied in [3, Fig. 6 (b)]. Here $\overline{\vartheta}$, $\Delta\vartheta$ are equivalent parameters, according to (21). The grating thickness t_g has been chosen equal to the period Λ and the simulation has been performed for a normal-incident TE plane-wave in the operating wavelength range $\lambda \in [1.3, 1.6]\Lambda$. The numerical results have been obtained with an in-house RCWA simulator by using $N_{pw} = 23$ plane waves to represent the grating modes.

Figure 5 shows the response of this grating versus $\overline{\vartheta}$ obtained with the RCWA (solid black curve) and with the expressions (22) and (24) for the parameter values indicated by the dot markers in Fig. 4. The agreement between the numerical and the analytic models is local mainly because of the dispersion of Ψ and $\Delta\vartheta$, whose effect on the position of the reflection peak is quantified by (25). Instead, the remaining parameters Θ and Φ exhibit a weak dependence on frequency. It can be noted that, in the proximity of $\overline{\vartheta} = 0.14\pi$ (magenta marker) and $\overline{\vartheta} = 0.93\pi$ (cyan marker), where a Fano resonance and a reflection zero are respectively occurring, the magenta and cyan curves are perfectly matching the numerical results. This shows the validity of this method in the characterization of narrow-band phenomena, such as resonances, as it will be discussed in great detail in Part II. The effect of dispersion will be introduced in the model in the third paper of this series.

From Fig. 5 it appears that the response is the superposition of two single-mode FPI contributions, in this case having low and high finesse, as suggested by (10) and (11). Their interference produces the transmission zero (100% reflection peak), which always exists as predicted by (25). The resulting quick zero-one transition is commonly referred to as a Fano resonance [18].

VII. Conclusion

The inspiration for this paper comes from the work of the group of Connie Chang-Hasnain [3]. There, extensive parametric investigations have been performed by means of a mode-matching technique, by changing the HCG geometry.

Those results emphasized the role of two-mode interference as the key physical mechanism of the HCG response. Starting from this observation, we developed a framework based on reducing the electromagnetic problem to the abstract bimodal FPI. The "mirrors" are characterized by 3×3 scattering matrices, which are unitary and symmetric under the hypothesis of absence of losses and reciprocity. The core of this approach is the physically-oriented parametrization of such matrices by means of six angles, which led to explicit expressions of all the relevant FPI parameters, including reflection/transmission zeros and poles. Our approach is not meant to substitute numerical simulations, but to complement them. In fact, the explicit expressions we derived allow to predict, rather than just to observe, all the features of interest and their interrelations. Despite its abstract nature, our framework can be applied to real world devices, such as HCGs, by extracting the model parameters in a single operating point, and the model will be accurate in its neighborhood. This requires just one computation of the junction scattering matrix by mode-matching. Remarkably, explicit formulas allow to perform this extraction without numerical methods. In Part II this approach will be applied to characterize HCGs as resonators, while a third paper will deal with their wide-band reflectivity features.

ACKNOWLEDGMENT

The authors gratefully thank prof. Fulvio Ricci for the fruitful suggestion of the parametrization of 3×3 symmetric unitary matrices.

REFERENCES

[1] W. Cauer, "Synthesis of linear communication networks," McGraw-Hill Book Company Inc., New York, Toronto, London, 1958.

[2] P. Hariharan, "Optical interferometry," *Elsevier,* Academic Press, 2003.

[3] C. J. Chang-Hasnain and W. Yang, "High-contrast gratings for integrated optoelectronics," *Adv. Opt. Photon.,* vol. 4, pp. 379-440, 2012.

[4] C. F. R. Mateus, M. C. Y. Huang, Y. Deng, A. R. Neureuther, and C. J. Chang-Hasnain, "Ultrabroadband mirror using low-index cladded subwavelength grating," *IEEE Photon. Technol. Lett.,* vol. 16, no. 2, pp. 518-520, Feb. 2004.

[5] C. J. Chang-Hasnain, Y. Zhou, M. C. Y. Huang, and C. Chase, "High-contrast grating VCSELs," *IEEE J. Sel. Topics Quantum Electron.,* vol. 15, no. 3, May/June 2009.

[6] P. Debernardi, R. Orta, T. Gründl, and M. C. Amann, "3-D vectorial optical model for high-contrast grating vertical-cavity surface-emitting lasers," *IEEE J. Quantum Electron.,* vol. 49, no. 2, pp. 137-145, Feb. 2013.

[7] C. Sciancalepore, B. B. Bakir, S. Menezo, X. Letartre, D. Bordel, and P. Viktorovitch, "III-V-on-Si photonic crystal vertical-cavity surface-emitting laser arrays for wavelength division multiplexing," *IEEE Photon. Technol. Lett.,* vol. 25, no. 12, pp. 1111-1113, June 2013.

[8] A. Liu, W. Hofmann, and D. H. Bimberg, "Two-dimensional analysis of finite size high-contrast gratings for applications in VCSELs," *Opt. Express,* vol. 22, no. 10, pp. 11804-11811, May 2014.

[9] M. Gebski, M. Dems, A. Szerling, M. Motyka, L. Marona, R. Kruszka, D. Urbańczyk, M. Walczakowski, N. Palka, A. Wójcik-Jedlińska, Q. J. Wang, D. H. Zhang, M. Bugajski, M. Wasiak, and T. Czyszanowski, "Monolithic high-index contrast grating: a material independent high-reflectance VCSEL mirror," *Opt. Express,* vol. 23, no. 9, pp. 11674-11686, May 2015.

[10] A. Tibaldi, P. Debernardi, and R. Orta "High-contrast gratings performance issues in tunable VCSELs," *IEEE J. Quantum Electron.* vol. 51, no. 12, Dec. 2015.

[11] V. Karagodsky, F. G. Sedgwick, and C. J. Chang-Hasnain, "Theoretical analysis of subwavelength high contrast grating reflectors," *Opt. Express,* vol. 18, no. 16, pp. 16973-16988, Aug. 2010.

[12] Y. Zhou, M. Moewe, J. Kern, M. C. Y. Huang, and C. J. Chang-Hasnain, "Surface-normal emission of a high-Q resonator using a subwavelength high-contrast grating," *Opt. Express,* vol. 16, no. 22, pp. 17282-17287.

[13] A. Taghizadeh, J. Mørk, and I.-S. Chung, "Ultracompact resonator with high quality-factor based on a hybrid grating structure," *Opt. Express*, vol. 23, no. 11, pp. 14913-14921.

[14] H. L. Bertoni, L.-H. S. Cheo, and T. Tamir, "Frequency-selective reflection and transmission by a periodic dielectric layer," *IEEE Trans. Antennas Propag.,* vol. 37, no. 1, pp. 78-83, Jan. 1989.

[15] A. Hessel and A. A. Oliner, "A new theory of Wood's anomalies on optical gratings," *Appl. Opt.,* vol. 4, no. 10, Oct. 1965.

[16] T. Tamir and S. Zhang, "Modal transmission-line theory of multilayered grating structures," *IEEE J. Lightw. Technol.,* vol. 14, no. 5, pp. 914-927, May 1996.

[17] S. S. Wang, R. Magnusson, J. S. Bagby, and M. G. Moharam, "Guided-mode resonances in planar dielectric-layer diffraction gratings," *J. Opt. Soc. Am. A,* vol. 7, no. 8, Aug. 1990.

[18] S. Fan, W. Suh, and J. D. Joannopoulos, "Temporal coupled-mode theory for the Fano resonance in optical resonators," *J. Opt. Soc. Am. A,* vol. 20, no. 3, pp. 569-572, Mar. 2003.

[19] K. Y. Bliokh, Y. P. Bliokh, V. Freilikher, S. Savel'ev, and F. Nori, "Unusual resonators: plasmonics, metamaterials and random media," *Rev. Mod. Phys.,* vol. 80, no. 4, pp. 1201-1213, Oct.-Dec. 2008.

[20] R. Magnusson and M. Shokooh-Saremi, "Physical basis for wideband resonant reflectors," *Opt. Express,* vol. 16, no. 5, pp. 3456-3462, Feb. 2008.

[21] A. Taflove and S. C. Hagness, "Computational electrodynamics: the finite-difference time-domain method," *Artech House Antennas and Propagation Library*, Artech House, III edition, 2013.

[22] G. Pelosi, A. Freni, and R. Coccioli, "Hybrid technique for analysing scattering from periodic structures," *IEE Proceedings H,* vol. 140, no. 2, pp. 65-70, Apr. 1993.

[23] A. Tibaldi, R. Orta, O. A. Peverini, G. Addamo, G. Virone, and R. Tascone, "Skew incidence plane-wave scattering from 2-D dielectric periodic structures: analysis by the mortar-element method," *IEEE Trans. Microw. Theory Techn.,* vol. 63, no. 1, pp. 11-19, Jan. 2015.

[24] M. G. Moharam and T. K. Gaylord, "Rigorous coupled-wave analysis of planar-grating diffraction," *J. Opt. Soc. Am.,* vol. 71, no. 7, pp. 811-818, July 1981.

[25] L. Li, "Use of Fourier series in the analysis of discontinuous periodic structures," *J. Opt. Soc. Am. A.,* vol. 13, no. 9, pp. 1870-1876, Sep. 1996.

[26] R. H. Morf, "Exponentially convergent and numerically efficient solution of Maxwell's equations for lamellar gratings," *J. Opt. Soc. Am. A,* vol. 12, no. 5, pp. 1043-1056, May 1995.

[27] O. A. Peverini, G. Addamo, R. Tascone, G. Virone, P. Cecchini, R. Mizzoni. F. Calignano, E. P. Ambrosio, D. Manfredi, and P. Fino "Enhanced topology of E-plane resonators for high-power satellite applications," *IEEE Trans. Microw. Theory Tech.,* vol. 63, no. 10, pp. 3361-3373, Oct. 2015.

[28] P. Sarasa, Á. Gonzáles, H. Esteban, P. Mader, K. Tossou, and P. Lepeltier, "Comparative study of the power handling capability of space broadband antenna filters in Ku-band," *MULCOPIM 2005,* ESTEC, Noordwijk, The Netherlands, 12-14 Sept. 2005.

[29] B. Gimeno and M. Guglielmi, "Full wave network representation for rectangular circular and elliptical to elliptical waveguide junctions," *IEEE Trans. Microw. Theory Tech.,* vol. 45, no. 3, pp. 376-384, Mar. 1997.

[30] P. Arcioni, M. Bressan, G. Conciauro, and L. Perregrini, "Wideband modeling of arbitrarily shaped E-plane waveguide components by the boundary integral-resonant mode expansion method," *IEEE Trans. Microw. Theory Tech.,* vol. 44, no. 11, pp. 2083-1092, Nov. 1996.

[31] O. A. Peverini, G. Addamo, G. Virone, R. Tascone, and R. Orta, "A spectral-element method for the analysis of 2-D waveguide devices with sharp edges and irregular shapes," *IEEE Trans. Microw. Theory Tech.,* vol. 59, no. 7, pp. 1685-1995, July 2011.

[32] P. Dita, "Parametrisation of unitary matrices," *J. Phys. A: Math. Gen.,* vol. 15, pp. 3465-3473, 1982.

[33] C. Jarlskog, "A recursive parametrization of unitary matrices," *J. Math. Phys.,* vol. 46, pp. 103508, Oct. 2005.

[34] C. Jarlskog, "Recursive parametrization and invariant phases of unitary matrices," *J. Math. Phys.,* vol. 47, pp. 013507, Jan. 2006.

[35] F. Ricci, Private communication, Scuola Normale Superiore, Pisa, Italy

Renato Orta (M'92-SM'99) is a member of the Department of Electronics, Politecnico di Torino, since 1974. He joined the Department as Assistant Professor, in 1987 became Associate Professor and since 1999 is Full Professor. He currently teaches courses on electromagnetic field theory and optical components. His research interests include the areas of microwave and optical components, radiation and scattering of waves and numerical techniques. He is Senior Member of the IEEE.

Alberto Tibaldi was born in Casale Monferrato, Italy, in 1987. In 2009, 2011 and 2015 he received the B.Sc., M.Sc. and Ph.D. degrees in Electronic Engineering from Politecnico di Torino. In 2012 he joins the Italian National Council of Research (CNR) as a research fellow. His scientific interests mainly regard numerical techniques applied to the modeling of electromagnetic passive components and to the electron transport analysis of semiconductor devices.

Pierluigi Debernardi was born in Casale Monferrato and received his degree in Electronics Engineering in 1987 from Politecnico di Torino, Italy. Since 1989 he's with the Italian National Council of Research at Politecnico di Torino. His interests are mainly in the field of the modeling of semiconductor materials and devices for optoelectronic applications. Recently he is mostly involved in modeling and designing VCSEL structures with non-circular and/or complex geometries, so as to achieve specific performances.